

Mechanical compliance of photolithographically defined vertically aligned carbon nanotube turf

C. M. McCarter · R. F. Richards · S. Dj. Mesarovic ·
C. D. Richards · D. F. Bahr · D. McClain ·
J. Jiao

Received: 8 August 2005 / Accepted: 18 January 2006 / Published online: 24 September 2006
© Springer Science+Business Media, LLC 2006

Abstract We describe the micro-mechanical properties of vertically aligned carbon nanotubes (VACNTs) fabricated using a photolithographically patterned iron catalyst prepared using sol–gel techniques. The carbon nanotubes (CNTs) were grown via chemical vapor deposition. The relative mechanical stiffness of the resultant structure was measured using nanoindentation based techniques and is shown to be related to the number of contact sites between tubes. Elastic deformation occurs during compression at large strains, however energy is dissipated during deformation, likely through tube–tube interactions. The effective elastic moduli are depth dependent, due to the compression of pre-buckled geometries. The effective elastic moduli range between 0.03 and 0.08 GPa for a low number of contact sites and 0.1 and 0.3 GPa for a high number of contact sites.

Introduction

Theoretical predictions of the properties of carbon nanotubes (CNTs) have shown some of the most desirable electrical, thermal and mechanical properties

of almost all known materials. These predictions have fueled a continually growing collection of theoretical and experimental studies of CNTs in the last 20 years [1–6]. While many of the properties of single CNTs, randomly aligned CNTs, and CNT composites have been reported [7–9], the vertically aligned carbon nanotube (VACNT) structure has not been well characterized. However, VACNTs are likely structures for use in microelectronic devices and microelectromechanical systems (MEMS) due to the relative ease of manufacture and ability to be integrated with MEMS structures for thermal control. The mixed scale nature of VACNTs provides the ability to bridge length scales from nanometers to 10's of microns. Since Terrones et al. grew the first VACNT structures in 1997 [10], several other research groups have demonstrated growth from catalysts on substrates; these usually consist of transition metal catalysts with growth via vapor deposition.

Although the mechanical properties of VACNT structures have been studied by other research groups, only the properties of individual tubes or the interaction of a few CNTs at a time have been examined to date [11–13]. In multi-scale applications, it is important to understand the mechanical response of many CNTs deforming with respect to one another. One multi-scale application that has become increasingly attractive is a MEMS thermal switch [14], which could be achieved using patterned VACNT structures. For this application, the MEMS structure will mechanically oscillate, alternatively contacting a hot surface and a cold surface to rapidly transfer heat with temporal and spatial control. Therefore, the VACNT structure will undergo compressive loading in the direction of growth. As the VACNT is a high aspect ratio structure, the possibility

C. M. McCarter · R. F. Richards · S. Dj. Mesarovic ·
C. D. Richards · D. F. Bahr (✉)
Mechanical and Materials Engineering,
Washington State University, Pullman, WA 99163, USA
e-mail: bahr@mail.wsu.edu

D. McClain · J. Jiao
Department of Physics, Portland State University,
Portland, OR 97207-0751, USA

of buckling during compressive loading may offset the exceptional stiffness measured in tension for individual CNTs [15] and in bending [16].

In this report, a method is described to fabricate patterned VACNT turf using processes and materials, which are compatible with common microelectronics and MEMS fabrication techniques, for eventual integration into a MEMS based thermal switch. The thermal switch [14] is actuated to make and break mechanical contact between a hot and cold surface; when in contact heat can transfer via conduction through the switch, therefore a compliant switch in compression is desired to ensure conformal contact along surfaces to overcome any surface asperities. To understand the response of an assembly of CNTs contacting a relatively large surface, a Berkovich diamond tip with an effective tip radius of $1.79\ \mu\text{m}$ was used to apply a load to the resulting VACNT structure.

Experimental

Preparation of patterned catalyst

The VACNT turf in this study were grown using chemical vapor deposition (CVD) with an iron catalyst dispersed in a glassy thin film deposited via spin coating onto silicon wafers using sol–gel chemistry. The sol–gel catalyst was made by combining 10 mL ethanol, 10 mL tetraethoxysilane (TEOS) (99.999+%, Alfa Aesar), 15 mL of a 0.7 M solution of iron nitrate (98+%, Alfa Aesar) and water ($\text{H}_2\text{O}:\text{Fe}(\text{NO}_3)_3$), and 2 drops of HNO_3 with magnetic stirring between each addition. This solution was then aged for 16 days. A (100) silicon wafer was prepared by removing the native oxide layer in a buffered oxide etchant (BOE) (4.5% HF, 36% Ammonium Fluoride, General Chemical). After removal of the oxide, the prepared silicon wafer was spin coated with the sol–gel catalyst solution at 3000 rpm for 30 s. The coated wafer was dried overnight at $80\ ^\circ\text{C}$ to create a thin glassy film. A commercially available photoresist, AZ 5214 (Clariant Corp.), was spun on, exposed to UV light through a mask, and developed in AZ 400 K (Clariant Corp.). The wafer was then immersed in BOE from 30–60 s to etch the catalyst containing film. The remaining photoresist was then removed with acetone before growth.

Growth of VACNT Turf

CNT growth followed the procedure originally described by L. Dong et al. [17]. The silicon die with patterned catalyst structures were placed in a tube

furnace, and the system was evacuated to 120 mTorr and catalyst film calcination was performed at $450\ ^\circ\text{C}$ for 120 min. Next, catalyst activation was performed at $500\ ^\circ\text{C}$ for 30 min and again at $600\ ^\circ\text{C}$ for 30 min while flowing H_2 (385 sccm) under a pressure of 75 Torr into the tube furnace. Finally, multi-walled carbon nanotube (MWCNT) growth occurred at $700\ ^\circ\text{C}$ for 30 min with an admixture of H_2 and C_2H_2 (385 sccm and 25 sccm, respectively) while maintaining the chamber pressure at 75 Torr. After growth, the system was cooled under vacuum to room temperature and then the samples were removed for analysis. A total of four different samples were grown in this study over a period of approximately 2 months, the order of growth was sample A, C, B, and D. During any given growth run the chamber pressure may fluctuate by up to 11 Torr.

Morphological characterization

After drying the photolithographically patterned sol–gel thin film, the samples were characterized with a Park Autoprobe CP atomic force microscope (AFM). After growth and after activation, samples were characterized using an FEI Sirion field emission scanning electron microscope (FESEM) and an FEI Tecnai F-20 field emission high resolution transmission electron microscope (TEM). For TEM sample preparation, a portion of the CNTs were removed from the silicon die and dispersed in acetone. Several drops of the suspension were then dropped onto a holey carbon TEM grid for individual tubes analysis. An available image processing program (Image SXM) was used to measure the catalyst particle size.

Nanoindentation of VACNT turf

Four silicon wafer die, labeled here as A, B, C and D, with patterned VACNT structures were mechanically tested using a Hysitron (Hysitron Inc., Minneapolis, MN) Triboscope nanoindentation system coupled to the Park Autoprobe CP. The methods outlined by Oliver and Pharr for improved nanoindentation analysis were used to calibrate the system and interpret the data [18]. The tip initially came into contact with the patterned CNT turf with a set point of $3\ \mu\text{N}$ (this position is considered the effective surface, or zero depth, in the following analysis). Indentation sites were chosen by moving the tip in intervals of $10\ \mu\text{m}$ in both the x and y directions, but without visualizing the surface of the VACNT turf in the Triboscope system to minimize the effects of wear. The sample was then

quasi-statically indented with maximum loads ranging from 50 μN to 100 μN .

The sample was also tested using a nanoindentation dynamic mechanical analyzer, sometimes referred to in the literature as the continuous stiffness method [18]. This technique employs the same basic hardware as the quasi-static technique; however, a sinusoidal modulation is added to the loading schedule using Hysitron's nanoDMA and the DSM 3.0 software package. This allows for multiple stiffness measurements to be made in one location as well as the ability to measure rate dependence. The sample was approached with a set point of 3.0 μN , and the indent site was located by moving the tip in the x and y directions at 10 μm intervals. The loading schedule in the continuous stiffness mode began at 30 μN and ended at 1,000 μN with a dynamic load of 10 μN , a loading rate of 100 $\mu\text{N/s}$, and a total of 30 segment steps. Two frequencies were used, 40 Hz and 60 Hz. However, no appreciable frequency dependence was observed over these ranges.

Results and discussion

Using the method described above to pattern the sol-gel catalyst, reproducible pattern features on the current mask as small as 5 μm were created; however, this is not the limit of the process. Any number of different photolithography techniques that have been used to pattern oxide films can be used to pattern the resulting film for aligned CNT growth. The surface of the sol-gel catalyst was analyzed using an AFM to locate possible catalyst particles precipitating from the glass before the activation step. However, the resulting glassy thin film was smooth and showed a consistent height of 500 nm, as measured using AFM and shown in Fig. 1.

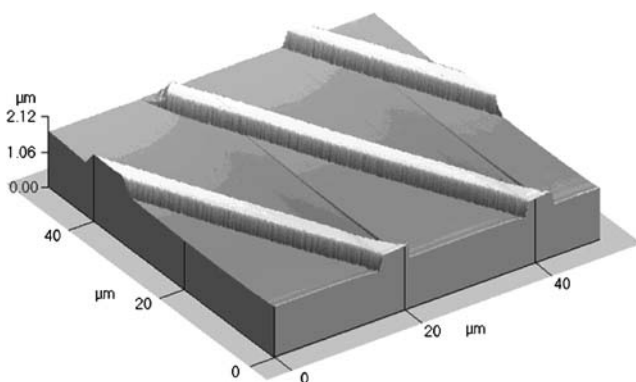


Fig. 1 After examination with an AFM, the patterned sol-gel catalyst was found to have a thickness of 500 nm. Also, the surface of the catalyst was smooth indicating that no iron precipitates were present before the catalyst activation step

As the sol-gel ages, before it is spun onto wafers, the ethanol-filled pores within the structure become smaller as the gel structure becomes more inter-connected. It is suspected that the catalyst particle size is related to the pore size. If sol-gel age is controlled, a prescribed pore size and therefore catalyst particle size could result. It has been shown that the catalyst particle size is related to the resulting CNT size [19, 20]. In this study, we are able to resolve the catalyst particles using SEM (Fig. 2).

The catalyst particle size is related to the resulting average CNT size, as shown in the inset of Fig. 2. The catalyst particles could be further controlled to give predictable sized particles depending on the heat treatment before growth, including calcination and catalyst activation. A longer heat treatment period or higher temperature will result in larger particles [21]. Future studies are directed toward controlling the catalyst particle size through sol-gel age and heat treatment for controlled CNT growth.

High resolution TEM imaging of dispersed CNTs from this growth process displays well-graphitized tubes with a multiwall configuration, as shown in Fig. 3a, with a mean diameter of 10 nm. Figure 3b is an FESEM image of a patterned VANCT turf structure. The structure shows growth only occurs on the patterned catalyst regions, with no evidence of CNT growth on the remainder of the substrate. The use of the sol-gel catalyst technique, as demonstrated here for patterning a VACNT turf, can be implemented in traditional microelectronic and MEMS processes

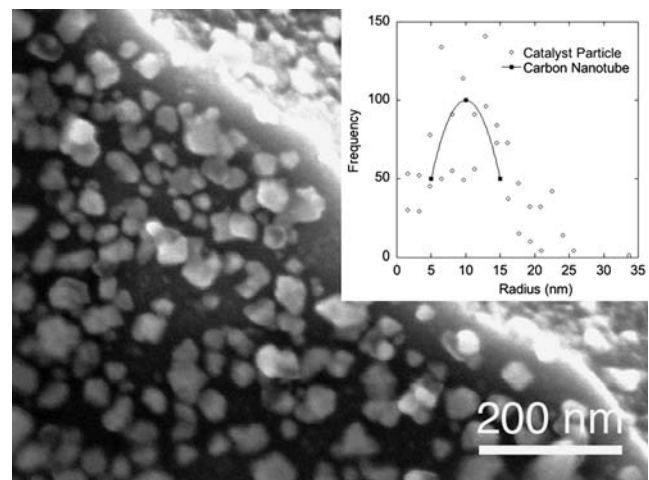


Fig. 2 The catalyst particles shown in the SEM image taken after catalyst activations support carbon nanotube growth. The size distribution of the catalyst particles is shown in the inset. The particle distribution was calculated using Image SXM, and plotted with the average carbon nanotube radius. The trend line shown in the inset is only present to guide the eye

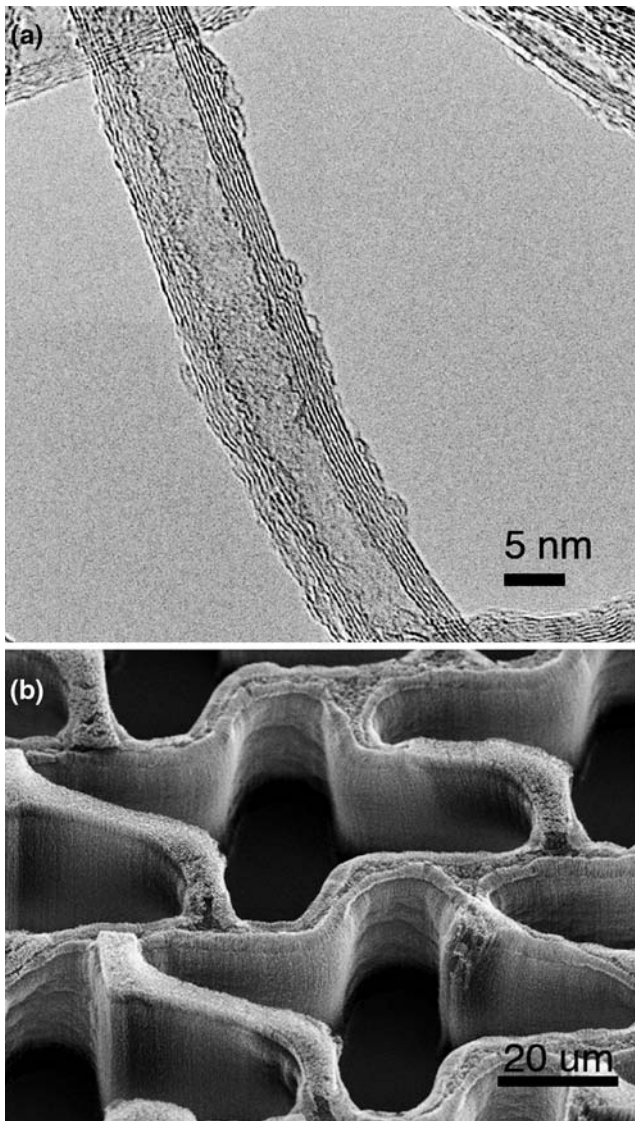


Fig. 3 (a) The HRTEM image shows the internal structure of a representative MWCNT for the four die studied in this letter. The image also reveals eight graphitic layers for this nanotube while MWCNTs in the VACNT turf generally display a distribution of between five and ten layers. (b) An FESEM image demonstrates the mask feature retention of VACNT with heights in excess of 20 μm

without additional development of photolithography techniques.

Of the four samples grown in this study, two exhibit a relatively convoluted “vertically-aligned” structure as shown in Fig. 4A and B and the other two, shown in Fig. 4C and D, exhibit a more aligned structure in the growth direction.

Within the same volume of sample imaged in Fig. 4, sample A had 82 points of contact, while sample C had 55 points of contact. The points of contact are defined as places where two or more CNTs come into or out of

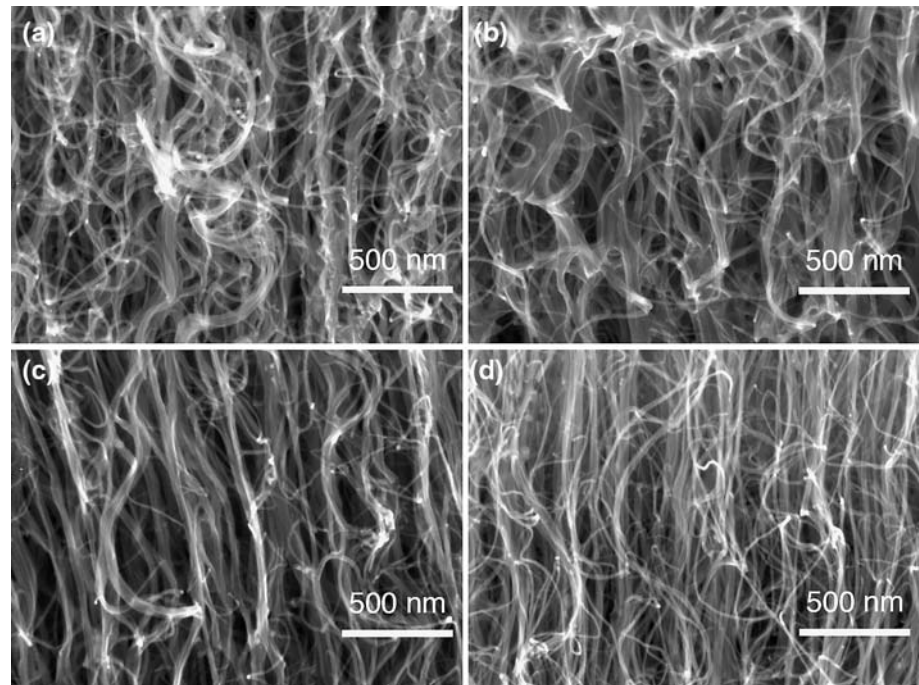
contact. These measurements should only be considered as a qualitative measure of the CNT–CNT interaction, but are effective for a first order approximation. A more accurate method for measuring the amount of contact between CNTs is being developed to further quantify this CNT–CNT interaction region. There would appear to be a relationship between the degree of alignment of the CNTs and the number of contact sites between the CNTs. In this study, we have found that “less aligned” CNTs have higher the number of contact sites than the “aligned” structures. In a related study, a model has been developed which demonstrates that the degree of contact or contact length is the characteristic property that will control the effective stiffness or elastic modulus of the VACNT turf (Mesarovic S. Dj. et al., submitted to Scripta Mater). The alignment of the CNTs is therefore related to mechanical compliance of the VACNT structure.

The VACNT turf is very compliant when tested in compression. A representative load depth curve for a quasi-static nanoindentation test is shown in Fig. 5.

There is hysteresis in the load depth curves that indicates some mechanical energy has been absorbed in the CNT structures, but the complete return to the initial position indicates that this deformation is completely elastic at these loads and depths. Also of interest is the adhesion of the CNTs to the tip, as exhibited by the “negative” load on the unloading portion of the nanoindentation test. At the end of the loading portion of the indent cycle, the tip is held at the peak load for a period of time to measure the tendency of material creep. The load applied to the indenter is carried by both the sample and the springs which support the tip in the indentation system. Therefore, at a constant applied load to the top of the tip, if significant creep occurs between the tip and the sample it manifests as a drop in load applied to the sample. Since the CNT turf is very compliant, this effect of spring constants in the system is exacerbated when compared to an indentation in a conventional material. The downward slope at the end of the unloading curve is indicative of the machine spring constant. Specific load–depth curves varied considerably from indent to indent. Most of this scatter is due to the structural variability of the surface of the VACNT turf, as shown in Fig. 3B.

Because the continuous stiffness method allows multiple tests at the same location and can reach depths greater than 5000 nm, most of the variance encountered in quasi-static testing due to structural variations was eliminated. Each sample was indented in eight different locations. There were 30 elastic modulus readings taken at each location. The eight

Fig. 4 VACNT in (A) and (B) clearly show a more entangled structure which gives rise to a higher occurrence of van der Waals bonding between tubes than (C) and (D). As the number of bonding sites between CNTs is higher for samples (A) and (B), a higher modulus is expected and is confirmed by the continuous stiffness measurements shown in Fig. 5



data sets were averaged into a single set for each die. The elastic modulus data from the continuous stiffness method is summarized in Fig. 6. The data show that the effective elastic modulus of the VACNT turf in this study on average is 0.10 GPa. One other thermal

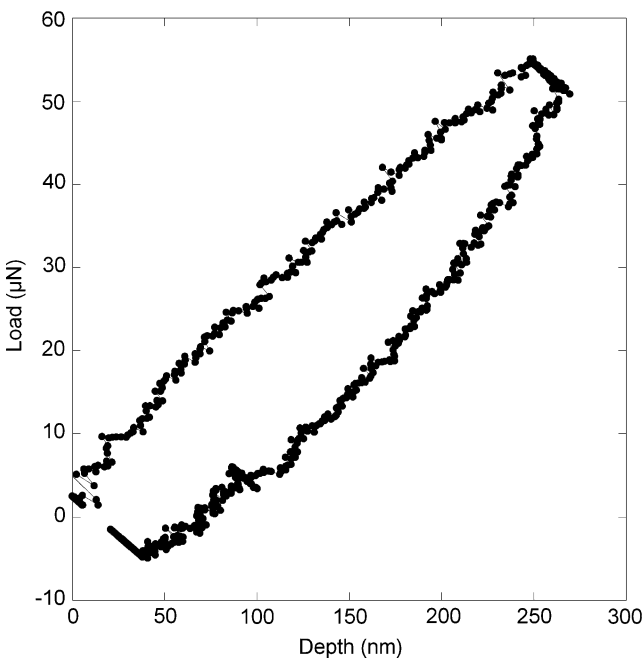


Fig. 5 The high compliance of the patterned VACNT turf is apparent from the high depth achieved with modest loads. The sample indented has an average CNT height of 2 μm . This load depth curve also shows hysteresis indicating absorption of energy by the VACNT turf, and a “pull off” force indicating adhesion between the tip and the aligned CNTs

switch structure, a mercury droplet array [14], has shown an effective elastic modulus of approximately 70 MPa by measuring the load–displacement relationship of the droplets between two flat plates. Low elastic moduli in compression are desired for a thermal switch so that conformal contact is ensured over rough contacting surfaces.

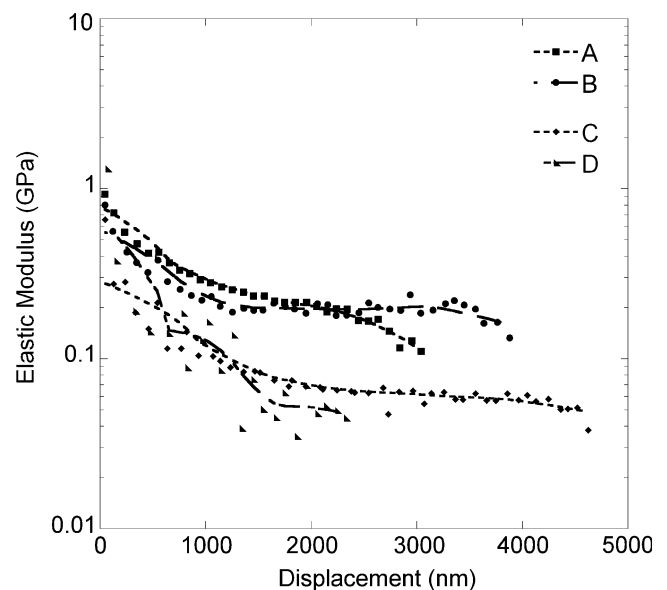


Fig. 6 The various VACNT turf structures show a clear distinction in effective elastic modulus from samples A and B to samples C and D. This is most likely due to the increased number of contacts between nanotubes in samples A and B. Eight modulus vs. depth curves were averaged for each die

Many of the published values for elastic properties of CNTs have demonstrated moduli in excess of 1000 GPa [15], significantly above the sub-GPa values measured in the current study. The difference between the current study and previous work is that the compression of a CNT is not equivalent to applying a tensile load on a straight structure. Instead, compression of assemblages of VACNT turf is effectively the elastic response of a pre-buckled structure (Mesarovic S. Dj. et al., submitted to *Scripta Mater*). One group has shown that multi-walled nanotubes have an elastic modulus ranging from 0.3–4 GPa when radially deformed, which strongly supports the radical anisotropy of the mechanical response of CNTs [22]. From Fig. 4, there are many points which appear to contact other tubes in the VACNT; these contacts may act as van der Waal bonding sites between CNTs. One significant finding of this work is that the VACNT turf with more points of contact between tubes has a higher average modulus. There are approximately twice the number of contacts in samples A and B than in samples C and D, with a corresponding increase in the effective elastic modulus. Increasing the density of CNTs and the amount of contact between CNTs increases the effective elastic modulus. Decreasing the density and the amount of contact decreases the effective modulus. It is likely that the catalyst morphology and growth conditions control the density and tortuosity of CNTs, and control of the catalyst morphology and growth conditions will result in predictable effective elastic moduli for a given VACNT structure.

These results are promising for the thermal switch application as the compliance of the CNT turf is comparable to the compliance of a previously fabricated thermal switch [14]. However, as different applications demand different properties, it is desirable to have a structure which could be more or less stiff than this average value. In addition to modifying this structure via the catalyst and growth, Kis et al. have shown that single wall nanotube bundles can be stiffened through electron irradiation, increasing the bending modulus up to thirty times the original value by tube “crosslinking” [23]. Therefore, it would seem reasonable to expect similar levels of control of the compliance of VACNT structures in future work.

Conclusions

For a VACNT thermal switching device, a compliant structure is preferred to allow conformal contact over a non-planar surface with minimal applied

loads. Following the fabrication methods outlined in this paper, a compliant patterned VACNT turf can be fabricated using traditional microelectronics processing techniques coupled with established methods of CNT growth. The effective elastic modulus measured with nanoindentation in this structure is low, on the order of 0.1 GPa. Moreover, it has been shown here that an increase in the number of CNT–CNT contact sites increases the stiffness in compression (the effective elastic modulus) during elastic loading. Therefore, it should be possible to tailor the compressive stiffness of VACNT turf structures depending on the level of tube entanglement and CNT–CNT contacts. Tube entanglement can likely be controlled through the control of catalyst preparation and growth conditions as well as post growth processes.

Acknowledgements The authors thank the National Science Foundation under grant number CTS-0404370 and the US Army SMDC under contract number DASG60-02-C-0084 for the financial support of this project.

References

1. Dresselhaus MS, Eklund PC (2000) *Adv Phys* 49:705
2. Berber S, Kwon YK, Tomanek D (2000) *Phys Rev Lett* 84:4613
3. Hone J, Batlogg B, Bener Z, Johnson AT, Fischer JE (2000) *Science* 289:1730
4. Shimizu T, Abe H, Ando A, Nakayama Y, Tokumoto H (2005) *Surf Interface Anal* 37:204
5. Kiang C-H, Goddard WA, Beyers R, Bethune DS (1995) *Carbon* 33:903
6. Mylvaganam K, Zhang LC (2004) *Carbon* 42:2025
7. Salvétat J-P, Kulik AJ, Bonard JM, Briggs GAD, Stockli T, Metenier K, Bonnamy S, Beguin F, Burnham NA, Forro L (1990) *Adv Mater* 11:161
8. Suhr J, Koratkar N, Koblinski P, Ajayan P (2005) *Nat Mater* 4:134
9. Demczyk BG, Wang YM, Cumings J, Hetman M, Han W, Zettl A, Ritchie RO (2002) *Mater Sci Eng A* 334:173
10. Terrones M, Grobert N, Olivares J, Zhang JP, Terrones H, Kordatos K, Hsu WK, Hare JP, Townsend PD, Prassides K, Cheetham AK, Kroto HW, Walton DRM (1997) *Nature* 388:52
11. Qi HJ, Teo KBK, Lau KKS, Boyce MC, Milne WI, Robertson J, Gleason KJ (2003) *Mech Phys Solids* 51:2213
12. Kinoshia H, Kume I, Tagawa M, Ohmae N (2004) *Appl Phys Lett* 85:2780
13. Poggi MA, Boyles JS, Bottomley LA, McFarland AW, Colton JS, Nguyen CV, Stevens RS, Lillehei PT (2004) *Nanoletters* 4:1009
14. Christensen AO, Jacob JP, Richards CD, Bahr DF, Richards RF (2003) In: Shoji S (ed) *The 12th International conference on solid state sensors, actuators and microsystems*, Boston, (IEEE 2003), p 1427
15. Yu M-F, Lourie O, Dyer MJ, Moloni K, Kelly TH, Ruoff RS (2000) *Science* 287:637

16. Demczyk BG, Wang YM, Cummings J, Hetman M, Han W, Zettl A, Ritchie RO (2002) *Mater Sci Eng A* 334:173
17. Dong L, Jiao J, Pan C, Tuggle DW (2004) *Appl Phys A* 78:9
18. Oliver WC, Pharr GM (1992) *J Mater Res* 7:1564
19. Cheung CL, Kurtz A, Park H, Lieber CM (2002) *J Phys Chem B* 106:2429
20. Ishida M, Hongo H, Nihey F, Ochiai Y (2004) *Jpn J Appl Phys* 43:L1356
21. Encheva G, Samuneva B, Djambaski P, Kashchieva E, Paneva D, Mitov I (2004) *J Non-Cryst Solids* 345,346:615
22. Yu M-F, Kowalewski T, Rouff RS (2000) *Phys Rev Lett* 85:1456
23. Kis A, Csanyi G, Salvétat J-P, Thien-Nga L, Couteau E, Kulik AJ, Benoit W, Brugger J, Forro L (2004) *Nat Mater* 3:153–157